Journal of Photochemistry and Photobiology A: Chemistry 217 (2011) 383–388

Contents lists available at ScienceDirect

Journal of Photochemistry and Photobiology A: Chemistry

journal homepage: www.elsevier.com/locate/jphotochem

Degradation of the herbicide 2,4-dichlorophenoxyacetic acid over TiO_2–CeO_2 sol–gel photocatalysts: Effect of the annealing temperature on the photoactivity

Félix Galindo-Hernández, Ricardo Gómez*

Universidad Autónoma Metropolitana-Iztapalapa, Department of Chemistry, San Rafael Atlixco 186, A. P. 55-534, México, D.F. 09340, Mexico

ARTICLE INFO

Article history:
Received 26 April 2010
Received in revised form 20 October 2010
Accepted 16 November 2010
Available online 24 November 2010

Keywords:
TiO_2–CeO_2 photocatalysts
Titanium deficiency
2,4-Dichlorophenoxyacetic acid photodegradation
Titania-ceria band gap
Titania-ceria Rietveld analysis

ABSTRACT

TiO_2–CeO_2 mixed oxides were synthesized by the sol–gel method and calcined at 473, 673 and 873 K. The preparation method enabled us to obtain TiO_2–CeO_2 mixed oxides with specific surface areas of 250, 174 and 99 m^2/g. An important effect of the thermal treatment on the band gap of the TiO_2–CeO_2 mixed oxides was observed. The E_g band gap shifts from 3.1 to 3.2 eV, for the TiO_2 bare catalysts, to 2.3–2.5 eV on the annealed mixed oxides. The X-ray Rietveld refinement shows that the calculated titanium deficiency diminishes as the annealing temperature of the mixed oxides is increased. A relationship between the titanium deficiency per unit cell (from 44.8 to 20.0%) the E_g band gap (2.3–2.5 eV) and the capacity for the herbicide photodegradation (from 85.6 to 94.5%) was observed.

1. Introduction

Titanium dioxide has attracted much attention as photocatalyst, because its textural, structural and semiconducting properties are all singular. Titanium dioxide is considered the semiconductor showing the best photoactivity. However, modifications in the anatase–rutile phase ratio, crystallite size, specific surface area, pore structure and band gap energy have important effects on its capacity to photodegrade the organic pollutants present in wastewater [1–4]. Improved titania-based photoactivity has been reported in solids whose photophysical and textural properties were modified by doping titanium dioxide with metals or metallic oxides [5,6]. In this way, important modifications in the titania network and hence in their structural and photocatalytic properties have been successfully obtained by means of the synthesis of doped titania materials using the sol–gel method. The sol–gel process allows doped-nanosized semiconductors formation by adding the doping metal precursor to the gelling titanium alkoxide solution [7–9]. In the sol–gel synthesis of the titanium alkoxide the hydrolysis and polycondensation reactions occur simultaneously forming higher molecular weight products [10–13]. The hydrolysis and polycondensation reactions are very sensitive to synthesis conditions such as the type and quantity of solvent, water concentration, pH of the gelling solution, reaction temperature and mixing conditions [14,15]. The effect of pH and cerium oxide content on the textural properties, crystalline structure and photophysical properties has been recently studied for TiO_2–CeO_2 semiconductors [16,17]. In such papers it has been reported that such properties are very sensitive to thermal treatments. When the annealing temperature of the solids was increased, a diminution in the titanium deficiency [V^{Ti+4}] was found. Also, by using electron density maps, a contraction of the titania network was observed. On the other hand, the photoactivity for the 2,4-dichlorophenoxiacetic acid on TiO_2–CeO_2 semiconductors annealed at constant temperature (673 K) was recently reported showing that the cerium oxide content modifies both the titania crystallite size and the photocatalytic properties [18].With the purpose to understand the role of the annealing temperature (473, 673 and 873 K) other than the cerium oxide content in the photocatalytic properties of TiO_2–CeO_2 mixed oxides the semiconductors were prepared by the sol–gel method using titanium isopropoxide and cerium nitrate as starting materials. The characterization of the TiO_2–CeO_2 solids annealed at different temperatures was performed by means of nitrogen adsorption, X-ray diffraction (XRD) Rietveld refinement and UV–Vis spectroscopy. The photocatalytic evaluation was carried out by degrading 2,4-dichlorophenoxyacetic acid.

2. Experimental

2.1. Catalyst preparation

The sol-gel TiO_2–CeO_2 material was synthesized at pH 3 using titanium alkoxide as reactant and HNO_3 as hydrolysis agent. The catalyst preparation process was as follows: to a 2 neck flask

* Corresponding author. Tel.: +52 55 58044668; fax: +52 55 58044666.
E-mail address: gomr@xanum.uam.mx (R. Gómez).

1010-6030/$ – see front matter © 2010 Elsevier B.V. All rights reserved.
doi:10.1016/j.jphotochem.2010.11.010

containing an ethanol/water solution (16:8 molar ratio), the appropriate amount of cerium nitrate (Aldrich 99.9%) to obtain 10 wt% CeO_2 in the final solids was added. Afterwards, 1 mol of titanium n-butoxide (Aldrich 97%) was added dropwise during 1 h. Then, the solution was maintained in reflux until the gel was formed. After gelling, the samples were dried in air at 373 K and annealed at 473, 673 and 873 K for 4 h using a program rate of 2 K/min.A TiO_2 bare sample calcined at 673 K was prepared in the same way described above but without adding cerium nitrate.

2.2. Characterization

2.2.1. Adsorption measurements

Nitrogen adsorption isotherms were obtained at 77 K with an automatic Quantachrome Autosorb 3B instrument. Prior to the nitrogen adsorption, all the samples were outgassed overnight at 573 K. The specific surface areas of the samples were calculated from the nitrogen adsorption isotherms using the BET method, and the mean pore size diameter form the desorption isotherms using the BJH method.

2.2.2. UV–Vis absorption spectra

The UV–Vis absorption spectra were obtained with a Varian Cary III UV–Vis spectrophotometer coupled with an integration sphere for diffuse reflectance studies. A sample of MgO with a 100% reflectance was used as a reference.

2.2.3. X-ray diffraction and Rietveld refinement

The X-ray diffraction patterns were obtained at room temperature with a Bruker Advance D-8 diffractometer with a Cu Kα radiation and a graphite secondary bean monochromator. The intensities were obtained in the 2 theta ranges between 20° and 100° with a step of 0.05° and a measuring time of 0.5 s per point. The crystalline structures were refined by Rietveld method [19–23]. The titania tetragonal structure was refined using a tetragonal unit cell with the symmetry described by group $I4_1/amd$. For the peak profile shapes, we used the Voigt function and the polynomial Cheby I whit 6 terms [24]. The values for titanium deficiency per unit cell (%) were calculated using the Wyckoff positions and the occupancies [23] were refined by the Rietveld method.

2.2.4. Electron density maps of Fourier

The electron density maps were calculated following the method described in detail elsewhere [17]. In brief, on a point (x, y, z) of the crystallite cell with volume V was calculated by Fourier series using the structural factors $F(h, k, l)$:

$$\rho(x, y, z) = V^{-1} \sum_h \sum_k \sum_l F(h, k, l) \exp[-2\pi i(hx + ky + lz)]$$

where (x, y, z) represents a vector r of real space, with one vector space (a, b, c) and (h, k, l) are the coordinates of one vector from the reciprocal space with base (a^*, b^*, c^*), i.e., they are the coordinates from the diffraction plane that it is given by Bragg's Law.

2.2.5. Catalytic activity

The photodegradation experiments were carried out at room temperature (298 K) as follows: to a flask with an aqueous solution (250 mL) containing 30 ppm of 2,4-dichlorophenoxyacetic acid, 250 mg of catalyst were added. The solution with air flux (Air-Pump BOYU S-4000B, Pressure: 0.012 MPa, Power: 9 W and OUTPUT: 3.2 l/min) was maintained under stirring for 15 min in the dark until reaching the adsorption–desorption equilibrium. Then, it was irradiated in a closed box with a UV lamp Pen-Ray (UVP), which emits a λ radiation of 254 nm with an emission of 2000 μW/cm^2. The reaction rate was followed by taking a sample every 15 min and then analyzed in a UV–Vis spectrophotometer Varian, model Cary-III. The concentration of 2,4-dichlorophenoxyacetic acid was calculated from the adsorption band at 229 nm, applying the Lambert–Beer equation.

Table 1
Specific surface areas and band gap energies for the TiO_2–CeO_2 samples annealed at different temperatures.

Sample	Surface area ($m^2\ g^{-1}$)	λ (nm)	E_g (eV)
TiO_2 at 673 K	73	388	3.1
TiO_2–CeO_2 at 473 K	250	539	2.3
TiO_2–CeO_2 at 673 K	174	517	2.4
TiO_2–CeO_2 at 873 K	99	496	2.5

E_g: band gap energy.

3. Results

3.1. Specific surface area

The specific surface areas of the samples annealed at different temperatures are reported in Table 1, where it can be seen that the BET specific surface area of titania-ceria decreases for the samples calcined at 473 and 873 K from 250 m^2/g to 99 m^2/g, respectively. This implies a diminution of 60% of the specific surface area by the effect of the annealing temperature; i.e., the pore walls were smoothed and some pores collapsed because of the sintering process [25]. Similar effects on the diminution of the specific surface area were also observed on TiO_2–CeO_2 samples prepared with different CeO_2 contents [18,25].

3.2. UV–Vis spectroscopy

The band gap energy (E_g) of the TiO_2, CeO_2 and TiO_2–CeO_2 samples calcined at 873 K was calculated from the UV absorption spectra (Fig. 1) by taking into account $\alpha(E)\ \alpha\ (E - E_g)^{m/2}$, where $\alpha(E)$ is the absorption coefficient for a photon with energy E, and $m = 1$ is for an indirect transition between bands [26]. The band gap energies calculated by a linear fit of the slope to the abscissa are reported in Table 1 for the titania–ceria mixed oxides. The E_g values for the titania–ceria mixed oxides are of the same order for the three annealing temperatures (2.3–2.5 eV), however, they are far from that obtained in the TiO_2 bare catalyst annealed at 673 K (3.2 eV) and that of CeO_2 (2.8 eV). In previous works, the E_g band

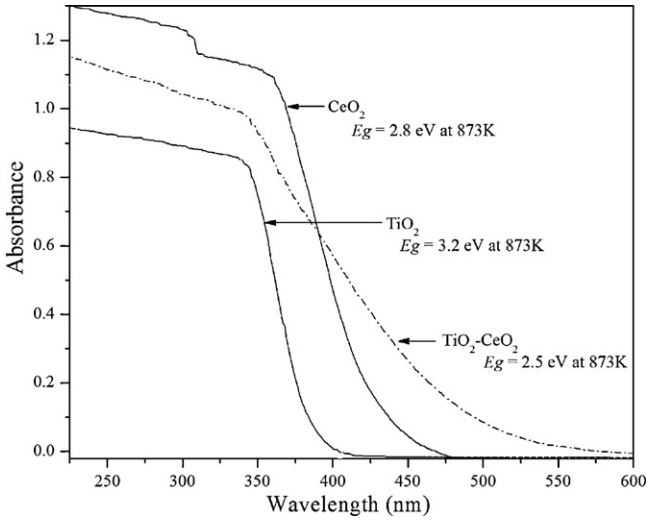

Fig. 1. UV–Vis spectra for the TiO_2, CeO_2 and TiO_2–CeO_2 samples annealed at the same temperature.

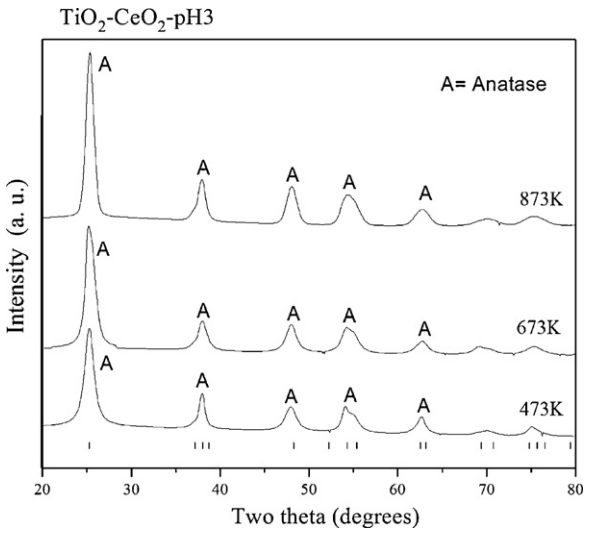

Fig. 2. Rietveld refinement plots for the TiO_2–CeO_2 samples as a function of the annealing temperature. Tick marks correspond to the anatase phase.

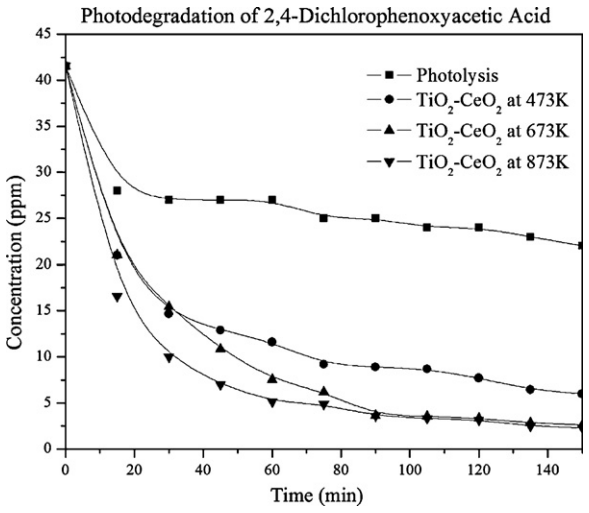

Fig. 4. Photodecomposition of the 2,4-dichlorophenoxyacetic acid on TiO_2–CeO_2 photocatalysts as a function of time.

Table 2
Rietveld refinement data for TiO_2–CeO_2 samples annealed at different temperatures.

Sample	Anatase (wt.%)	Crystallite size (nm)	$[V^{+}_{Ti}{}^{4+}]$
TiO_2–CeO_2 at 473 K	100	8.9 (7)	44.8
TiO_2–CeO_2 at 673 K	100	21.0 (10.3)	22.4
TiO_2–CeO_2 at 873 K	100	43.6 (2)	20.0

The number in parenthesis corresponds to the standard deviation.
$[V^{+}_{Ti}{}^{4+}]$: titanium deficiency per unit cell (%).

gap shift to the visible region has been attributed to the incorporation of Ce^{4+} cations substituting some Ti^{4+} cations in the titania network as well as by the titanium deficiency created per unit cell $[V^{+}_{Ti}{}^{4+}]$ [18,25].

3.3. X-ray diffraction patterns

The Rietveld refinement plots for the TiO_2–CeO_2 photocatalyst (Fig. 2) show anatase as the crystalline phase for all the samples. The absence of peaks identifying cerium oxide suggests the probable insertion of some Ce^{4+} in the titania network as well as the formation of cerium oxide conglomerates highly dispersed over the titania surface. The size of such conglomerates is too small and they cannot be detected because of the limited resolution obtained by XRD diffraction when supported nanocrystalline structures are present. In previous work on TiO_2–CeO_2 mixed oxides, the CeO_2 crystalline structure was identified in samples annealed up to 1073 K [25].

The crystalline size calculated by the Rietveld refinement for the various solids is reported in Table 2. The smallest nanocrystallites (8.9 nm) correspond to the sample annealed at 473 K; meanwhile the largest crystallite size (43.6 nm) was obtained in the sample annealed at 873 K.

The estimated values concerning the titanium deficiency per unit cell are reported in Table 2. It can be seen that it diminishes from 44.8 to 20% per unit cell on the TiO_2–CeO_2 photocatalyst calcined at 473 and 873 K, respectively. These results show that titanium deficiency can be created on TiO_2–CeO_2 mixed oxides by varying the annealing temperature of the xerogels.

The effect of the cerium oxide in the electron density of TiO_2 is illustrated in Fig. 3, where the electron density maps are very different for TiO_2 and TiO_2–CeO_2 semiconductors. These results suggest that the CeO_2 can modify the E_g band energy on the TiO_2–CeO_2 mixed oxides.

3.4. Catalytic activity

The activity of the catalysts was evaluated in the photodegradation of the 2,4-dichlorophenoxyacetic acid at room temperature. The photodegradation of the substrate was followed by the UV absorption band at 229 nm. The evolution of the 2,4-dichlorophenoxyacetic decomposition as a function of time is presented in Fig. 4. From the data in these curves, the apparent rate constant (K) was calculated by the Integral Method for an irreversible monomolecular first order reaction [26,27]:

$$-r_A = -\frac{dC_A}{dt} = KC_A$$

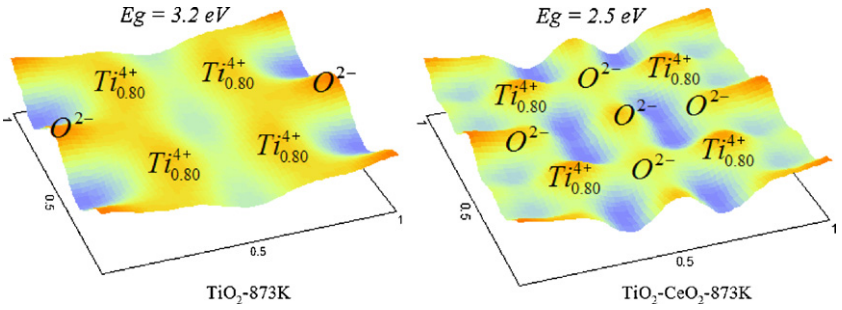

Fig. 3. Electron density maps of Fourier obtained by XRD for TiO_2 and TiO_2–CeO_2 samples annealed at 873 K.

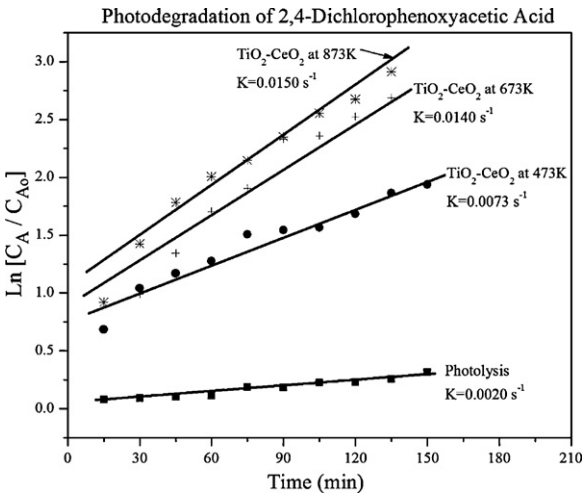

Fig. 5. Kinetic constant for the 2,4-dichlorophenoxyacetic acid decomposition on TiO_2–CeO_2 photocatalysts.

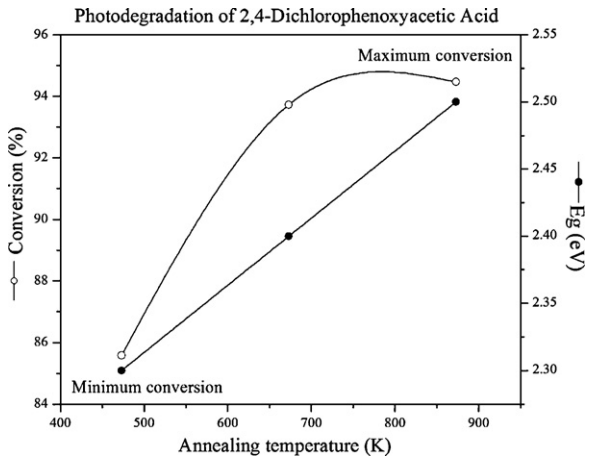

Fig. 6. Conversion and band gap energy as a function of the annealing temperature for the TiO_2–CeO_2 photocatalysts.

If the batch reactor works at constant density, then:

$$\ln\left[\frac{C_A}{C_{Ao}}\right] = -kt$$

where C_A is the concentration at time t, and C_{Ao} is the initial concentration.

An acceptable linearity was obtained by applying the first order kinetic equation (Fig. 5). The calculated values for the constant rate are reported in Table 3, where it can be seen that the highest value corresponds to the samples annealed at 873K ($k = 0.0150\ s^{-1}$). Although Fig. 4 shows some differences between the photoactivity of the TiO_2–CeO_2 materials annealed at 673 and 873 K, the mathematic treatment done over the experimental data by linear regression decreased the experimental error. In such a way the kinetic constant value for both samples appear to be the same (see Table 3).

The dependence of the photocatalytic activity and the photophysical properties (E_g) is presented in Fig. 6. An acceptable correspondence between the photoactivity and the band gap energy can be seen. It can be said that the E_g variation induced by the thermal treatments is the most important factor altering the photoactivity.

In Fig. 7, the photoactivity and the titanium deficiency, as a function of the annealing temperature, are presented. This figure shows that the catalyst with the lowest titanium deficiency is the most active for the 2,4-D photodegradation.

The TiO_2 is a dielectric material when it has a stoichiometric composition, i.e. the TiO_2 can become a semiconductor material when its stoichiometric composition is modified. The non-stoichiometric composition in the titania framework ($Ti_{1-x}O_2$) can be due to the point defects (Frenkel defects and/or Schotty defects) and/or substitutions during the syntheses process of the materials [28,29]. On the other hand, 3.1 and 3.20 eV values of band gap energy for TiO_2 solids synthesized by sol–gel method and annealed at 673 K and 873 K respectively have been reported [30–32]. In such a way these values have showed that band gap energy were not strongly dependent on the annealing temperature for TiO_2. Meanwhile in Table 1 and Figs. 1 and 3 show the important role of the cerium oxide in the band gap energy values (from 2.3 to 2.5 eV) in TiO_2–CeO_2 sol–gel. This result has been attributed to doping effects, some substitutions of Ti^{4+} by Ce^{4+} cations in the titania framework that form Ti–O–Ce bonds are reported [25]. The modification of the E_g band for the TiO_2–CeO_2 mixed oxides could also be a consequence of the transitions $f \rightarrow d$ of Ce^{3+} species and interband transitions in CeO_2 [33,34].

The titanium deficiencies, calculated by the Rietveld refinement method are point defects into the titania–ceria framework [28]. As a consequence, the electronic density can be modified by this fact in the TiO_2–CeO_2 solids (see Fig. 3). We can see these changes quantitatively on the band gap energy values reported in Table 1. On the other hand, the point defects are diminished by the increase in the crystallite size as consequence of the annealing temperature. This fact is due to the reorientation that the atoms acquire during calcination process, i.e. more of the amorphous parts of the TiO_2–CeO_2 solids are crystallized when the temperature is raised. Therefore at higher annealing temperature TiO_2–CeO_2 solids have better crystallinity and hence lower point defects.

Table 3
Photoactivity for the 2,4-dichlorophenoxyacetic acid decomposition on the TiO_2–CeO_2 samples annealed at different temperatures.

Sample	K (s^{-1})	Conversion after 2.5 h (%)
TiO_2	0.0020	53.0
TiO_2–CeO_2 at 473 K	0.0073	85.6
TiO_2–CeO_2 at 673 K	0.0140	93.7
TiO_2–CeO_2 at 873 K	0.0150	94.5

K: kinetic constant.

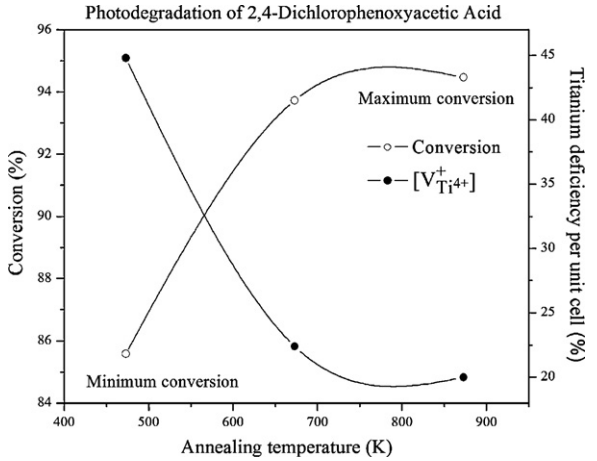

Fig. 7. Conversion and titanium deficiency as a function of the annealing temperature for the TiO_2–CeO_2 photocatalysts.

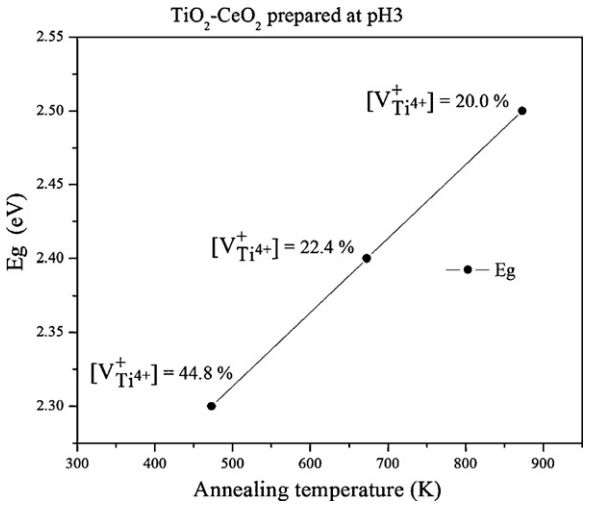

Fig. 8. E_g band gap and titanium deficiency as a function of the annealing temperature for the TiO_2–CeO_2 photocatalysts.

The titanium deficiency results were estimated from the occupancy calculated and the occupancy refined by Rietveld's technique as follows:

$$Occupancy\_calculated = \frac{Multiplicity\_of\_ion}{Maximun\_multiplicity\_for\_its\_space\_group}$$

$$Deficiency = \left[\frac{Occupancy\_calculated - Occupancy\_refined}{Occupancy\_calculated}\right] \times 100\%$$

It must be expected that in samples with a high titanium deficiency (see Table 2), important modifications in the band gap must be created. In Table 1, it can be seen that the lowest E_g value corresponds to the semiconductor with the highest titanium deficiency. However, when the semiconductor strongly diminishes the band gap, not only a fast electron–hole pair formation occurs; also a fast electron–hole recombination is produced at the same time. In Fig. 7 the photoactivity and titanium deficiency as a function of the annealing temperature is showed. In samples with a high titanium deficiency in which a fast electron–hole pair recombination must occur the photodegradation rate is diminished. Thus, an inverse correlation between the E_g band gap and titanium deficiency was obtained in the TiO_2–CeO_2 mixed oxides (Fig. 8). It should be noted, that the values of deficiencies shown in Table 2 are not necessarily

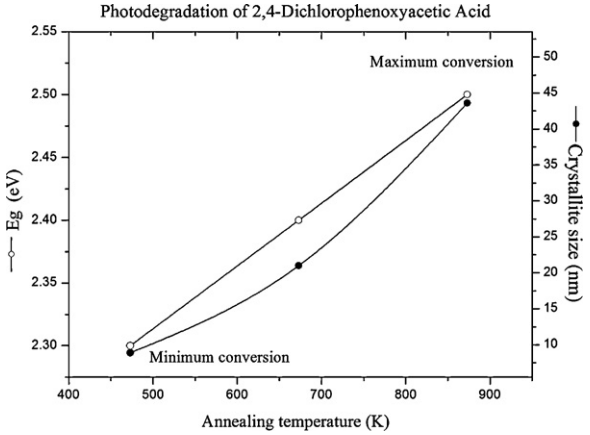

Fig. 9. Conversion and average crystallite size as a function of the annealing temperature for the TiO_2–CeO_2 photocatalysts.

titanium vacancies, i.e. the deficiencies of the Ti can be occupied by other ions as: oxygen and /or cerium [18].

Finally, the effect of the crystallite size on the photochemical properties of the TiO_2–CeO_2 semiconductors can be seen in Fig. 9. These results show that in TiO_2–CeO_2 semiconductors, modifications in the crystallite size and hence in the E_g can be produced by thermal treatments.

4. Conclusions

The present study shows the modifications in the textural, photophysical and photocatalytic properties induced by the annealing temperature on TiO_2–CeO_2 semiconductors: i) modification of the E_g band gap. ii) formation of strong titanium deficiencies [$V^{+}_{Ti}{}^{4+}$] in the solids. iii) important modifications in the crystallite size (8.9–43.6 nm). iv) important relationship between the photoactivity and the electron–hole pair recombination. It can be concluded that the band gap energy variations are a consequence of the titanium deficiency produced by the annealing temperature. These important factors E_g and titanium deficiency remarkably modifies the photocatalytic activity for the 2,4-D degradation on TiO_2–CeO_2 semiconductors.

Acknowledgements

F. Galindo thanks CONACYT for the postgraduate fellowship. This research was supported by the CONACYT-SEP grant 62053 ECO- CATALYSIS project.

References

[1] J.C. Yu, J.G. Yu, W.K. Ho, L.Z. Zhang, Chem. Commun. (2001) 1942.
[2] J.C. Yu, J.G. Yu, W.K. Ho, J.C. Zhao, J. Photochem. Photobiol. A 148 (2002) 263.
[3] J.G. Yu, J.C. Yu, W.K. Ho, Z.T. Jiang, New J. Chem. 26 (2002) 607.
[4] A. Fujishima, T.N. Rao, D.A. Tryk, J. Photochem. Photobiol. C 1 (2000) 1.
[5] J.M. Coronado, A.J. Maira, A. Martínez-Arias, J.C. Conesa, J. Soria, J. Photochem. Photobiol. A: Chem. 150 (2002) 213.
[6] Yue-Hua Xu, Zhuo-Xian Zeng, J. Mol. Catal. A: Chem. 279 (2008) 77.
[7] K.N.P. Kumer, K. Keizer, A.J. Burggraaf, T. Okubo, H. Nagamoto, S. Morooka, Nature 358 (1992) 48.
[8] S. Ito, S. Inoue, H. Kawada, M. Hara, M. Iwasaki, H. Tada, J. Colloid Interface Sci. 216 (1999) 59.
[9] G.W. Koebrugge, L. Winnubst, A.J. Burggraaf, J. Mater. Chem. 3 (1993) 1095.
[10] K. Terabe, K. Kato, H. Miyazaki, S. Yamaguchi, A. Imai, Y. Iguchi, J. Mater. Sci. 29 (1994) 1617.
[11] B.E. Yoldas, J. Mater. Sci. 21 (1986) 1087.
[12] H.K. Bowen, Mater. Sci. Eng. 65 (1986) 1574.
[13] J.S. Chappell, L.J. Procopio, J.D. Birchall, J. Mater. Sci. Lett. 9 (1990) 1329.
[14] D.Q. Fei, T. Hudaya, A.A. Adesina, Catal. Commun. 6 (2005) 253.
[15] J.F. Stebbins, Chem. Mater. 19 (2007) 1862.
[16] F. Galindo-Hernández, R. Gomez, J. Nano Res. 5 (2009) 87.
[17] F. Galindo-Hernández, R. Gómez, G. del Angel, C. Guzmán, J. Ceramic Proc. Res. 9 (2008) 616.
[18] F. Galindo, R. Gómez, M. Aguilar, J. Mol. Catal. A: Chem. 281 (2008) 119.
[19] IUCR, Powder Diffraction 22 21 (1997).
[20] C.J. Howard, J. Appl. Cryst. 15 615 (1982).
[21] A. Le Bail, H. Duroy, J.L. Fourquet, Mater. Res. Bull. 23 (1998) 447.
[22] http://www.ccp14.ac.uk.
[23] T. Hann, International Tables for Crystallography, vol. A, second edition, Kluwer Academic Publishers, 1989.
[24] M. Magini, A. Cabrini, J. Appl. Cryst. 5 (1972) 14.
[25] T. Lopez, F. Rojas, R. Alexander-Katz, F. Galindo, A. Balankin, A. Buljan, J. Solid State Chem. 177 (2004) 1873.
[26] N. Serpone, E. Pelizetti, Photocatalyst: Fundamentals and Applications, John Wiley, New York, 1989, pp. 60–61.
[27] O. Levenspiel, Chemical Reaction Engineering, John Wiley & Sons, Inc, New York, 1990, 50 p.
[28] F. Agullo-López, C.R.A. Catlow, P.D. Towsend, Point Defects in Materials, Academic Press, U.S.E, 1988, Chap. 1.
[29] C. Kittel, Introduction to Solid State Physics, 7th ed., John Wiley and Sons, Inc., New York, 1996, Chap. 18.

[30] X. Bokhimi, A. Morales, O. Novaro, T. López, E. Sanchez, R. Gomez, J. Mater. Sci. Res. 10 (1995) 2788.
[31] E. Sanchez, T. Lopez, R. Gomez, X. Bokhimi, A. Morales, O. Novaro, J. Solid Sate Chem. 122 (1996) 309.
[32] T. López, J. Hernandez-Ventura, R. Gómez, F. Tzompantzi, E. Sánchez, X. Bokhimi, A. Garcia, J. Molec. Catal. A: Chem. 167 (2001) 101.
[33] A. Bensalem, J.C. Muller, F. Bozon-Verduraz, J. Chem. Soc., Faraday Trans. 88 (1992) 153.
[34] G. Ranga Rao, H. Ranjan Sahu, Proc. Indian Acad. Sci. (Chem. Sci.) 113 (2001) 651.